Nuclear and Emerging Technologies for Space, American Nuclear Society Topical Meeting
Richland, WA, February 25 – February 28, 2019, available online at http://anstd.ans.org/

THERMAL-HYDRAULIC DESIGN FEATURES OF A MICRO NUCLEAR REACTOR POWER SOURCE APPLIED FOR MULTI-PURPOSE

Xiao Liu [1,2], Simiao Tang [1,2], Chenglong Wang [1,2]*, Wenxi Tian [1,2], Suizheng Qiu [1,2], Guanghui Su [1,2]*

[1] *Department of Nuclear Science and Technology, Xi'an Jiaotong University, Xi'an, Shaanxi, 710049, China*

[2] *Shaanxi Key Lab. of Advanced Nuclear Energy and Technology, Xi'an Jiaotong University, China*

Micro heat pipe cooled reactor power source (HRP) could be applied for space or underwater vehicles and it meets the future demands of them, safer structure, longer operating time, fewer mechanical moving parts than conventional power devices. In this paper, a 50kWe potassium heat pipe cooled reactor power source system is proposed. The reactor core is featured with Uranium nitride fuel and potassium heat pipes. Tungsten and water are used as shields and the reactivity is controlled by control drums. The thermoelectric generator (TEG) consists of thermoelectric conversion units and water cooler. The thermoelectric conversion units convert thermal energy to electric energy through the high-performance thermoelectric material. A code applied for designing and analyzing the rector power system is developed. It consists of multi-channel rector core model, heat pipe model using thermal resistance network, thermoelectric conversion and thermal conductivity model. Then the sensitivity analysis is performed on two key parameters of the designed micro-nuclear power source and the steady-state calculations are also conducted. It is concluded that the preliminary design of HPR design is reasonable and reliable. The designed residual heat removal system has sufficient safety margin to release the decay heat of the reactor. This work provides reference to the design of heat pipe cooled micro nuclear power source.

I. Introduction

Micro nuclear power source has a variety of applications like the energy systems of space station and underwater vehicles. More compact structure, longer operating time, higher energy density, fewer mechanical moving parts and higher reliability will meet the demands of future space station and underwater vehicle power system [1]. Compared with storage battery and fuel cell micro nuclear power source is a better way to realize these demands.

Micro-nuclear reactors applied for space station have been extensively researched in recent years. Various micro heat pipe cooled reactor power sources for space missions have been designed in the United States. Lithium and potassium heat pipe cooled reactor power source, MSR [2] , is designed for Martian surface power sources featured with thermal power of 1.2MWt and electrical power of 120kWe. The Heatpipe-operated Mars Exploration Reactor (HOMER) [3], featured with UN or UO2 fission fuel, is designed space station, and generated electrical power by Stirling engine whose conversion efficiency more than 20%. Sodium heat pipe cooled fast reactor, SAIRS [4], is controlled by drums featured with alkali metal thermoelectric converter and provide 100kWe electrical power for space station. And its thermoelectric conversion efficiency reaches more than 30%. HP-STMCS [5], producing 110kWe electrical power, controlled by control drums and cooled by lithium heat pipe is operated with Thermoelectric Module Converters. Prometheus [6], a gas (He-Xe) cooled reactor system characterized by Brayton cycle and water heat pipes for its radiator, produce 400-800kWt electrical power.

A micro nuclear reactor power source typical of 50kWe electrical power and a lifespan more than 10 years is conceptual designed [7]. It is featured with potassium heat pipes cooled core controlled by drums, and thermoelectric conversion technology with conversion efficiency reaching 10%. In this paper, a code for numerical simulating the nuclear micro power system is developed. Steady-state condition operating parameters are analyzed and simulated.

II. System Description

Reactor core, control drums, shield, heat pipes, thermoelectric generator (TEG) and seawater cooler are conceptual designed, shown in Fig.1. The core of HRP is a fast reactor with thermal power of 0.5MWt, and its detail structure is shown in Fig.2. UN cermet fission fuel with 45% enrichment of ^{235}U is adopted. In this core, potassium heat pipe with working temperature more than 700K is adopted as the main cooling method. 90 fuel rods and 37 heat pipes are arranged in a triangle array into a hexagon Nb-1Zr alloy matrix. The matrix is located in the center of a barrel whose inner surface is coated of Gd_2O_3 burnable poison. The barrel is surrounded by 6 control drums with $^{10}B_4C$ neutron absorber material. A cylinder Mo-14Re alloy vessel stores the reactor core. In the designed HRP, tungsten and water are arranged besides both sides of reactor as shields for γ ray and neutrons. Heat pipes pass through the shield and are inserted into the TEG, which converts heat from heat pipes into electricity of about 50kWe. And the seawater cooler is a

part device of the TEG, through which the coolant flows to remove waste heat.

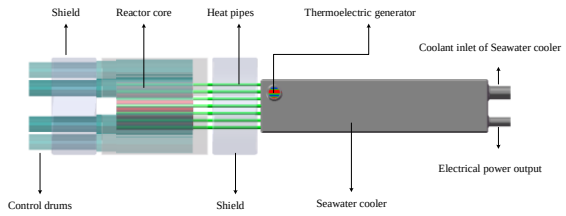

Fig. 1 Structure of micro nuclear reactor power source

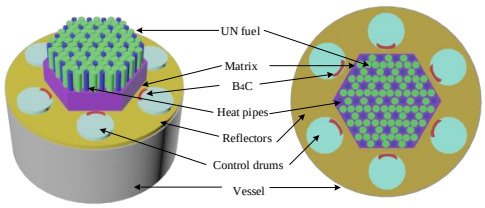

Fig. 2 Structure of HRP reactor core

The parameters shown in Table 1 are the system specification.

TABLE 1. micro-nuclear reactor power source system specifications

Parameters	Value	Unit
Thermal power	0.5	MWt
Core diameter	43.2	cm
Height of active zone	34	cm
Edge length of matrix	24.7	cm
Fuel radius	1.73	cm
Heat pipe radius	1.3	cm
Heat pipe wall thickness	0.5	mm
Heat pipe wick thickness	1	mm
Heat pipe evaporation section length	37	cm
Heat pipe length	1.85	m
Reflector thickness	8.6~10.3	cm
Edge length of TEG Stainless steel housing	53	cm

III. Numerical Model and Method

III.A. Reactor model

The reactor core can be divided into 37 single-cell units（shown in Fig.3）combined the fuel rods with the heat pipe. In order to accurately predict the power and temperature distribution of the core, one-sixth of the core is modeled according to symmetry. And it is divided into six channels corresponding one heat pipe with three surrounding fuel rods.

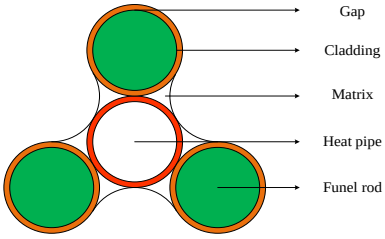

Fig. 3 A schematic view of the fuel unit

III.A.1. Reactor kinetics

Fission and decay power are included in heat generation in a nuclear reactor. the core fission power variation is calculated by the reactor point kinetics equations with six-family delayed neutrons. What's more, external reactivity insertion and incorporates reactivity feedback due to Doppler and temperature effects are considered. The point-kinetics equations are as follow:

$$\frac{dC_i}{dt} = \frac{\beta_i}{\Lambda} n - \lambda_i C_i \tag{1}$$

$$\rho(t) = \rho_a(t) + \sum \rho_i(t) \tag{2}$$

The first term $\rho(t)$ in Eq. (2) is the external reactivity. it presents the reactivity provided by the control drums and difference of material is input to the nuclear reactor core. The terms, $\rho_a(t)$ and $\sum \rho_i(t)$, are the reactivity feedback due to temperature reactivity feedbacks in different regions of the matrix. The temperature reactivity feedbacks are linear, where T_{FUEL} is the fuel average temperature.

$$\rho_{FUEL} = 0.02886 - 1.51289 \times T_{FUEL} \tag{3}$$

III.A.2. Heat transfer in the fuel unit

It can be seen from the above that the core structure of fuel unit is quite complicated. There are three layers of solid materials from the fuel rods to the wall of heat pipes. Meanwhile, in order to simplify the calculation, the core single-cell units can be regarded as a cylindrical channel by volume equivalent method (shown in Fig.4). The fuel units' radial control volume is shown in Figure 6.

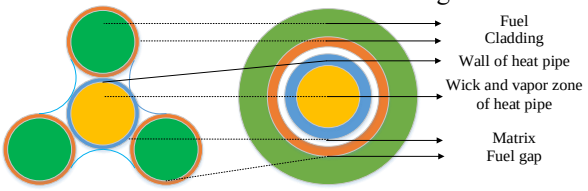

Fig. 4 Schematic of the fuel cell equivalent

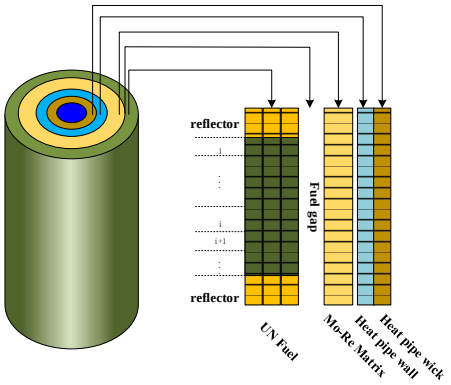

Fig. 5 The radial control volume of the fuel cell equivalent

Each reactor thermal model coupled to the heat pipes' heat transfer represents a single fuel unit, and the outer surface of the fuel unit is considered as adiabatic surface. The outer diameter of the matrix is determined by the average equivalent area per channel of reactor core. Heat conduction of all areas in the unit are considered, such as fuel rods, cladding, matrix and heat pipe wall. The internal heat source is considered to be the fission heat of fuel. The heat conduction model is based upon cylindrical coordinate system, without considering axial heat conduction. The heat conduction equations for all structures are as follows:

Fuel:

$$\rho_u c_u \frac{\partial T_u}{\partial t} = \frac{1}{r}\frac{\partial}{\partial r}\left(k_u r \frac{\partial T_u}{\partial r}\right) + Q_V \qquad (4)$$

Matrix:

$$\rho_M c_M \frac{\partial T_M}{\partial t} = \frac{1}{r}\frac{\partial}{\partial r}\left(\lambda_M r \frac{\partial T_M}{\partial r}\right) \qquad (5)$$

The gas conduction and radiation of gas heat transfer are considered when calculating the fuel gap heat transfer between fuel rods and matrix.

III.A.3. Heat transfer in the fuel unit

The heat transfer from the heat source (fission heat in the core) to the cold source (TEG) mainly relies on the following simultaneous and interrelated processes inside heat pipe: (1) radial heat conduction of wick (along with liquid) in evaporation section of heat pipe, RE_w (as shown in Fig.7); (2) radial heat conduction of wall in evaporation section, RE_s ; (3) axial heat transfer of potassium vapor, Rp; (4) radial heat conduction of wick (along with liquid) in condensation section, RC_w; (5) radial heat conduction of wall in condensation section, RC_s . In order to calculate the axial temperature distribution of the heat pipe, the evaporation section and the condensation section of the heat pipe are divided into several control volumes. The equivalent thermal resistance of each process is as follows:

Radial thermal resistance of the evaporation section:

$$R_{Es} = \frac{\ln(d_0/d_i)}{2\pi\lambda_w L_1} \qquad (6)$$

Evaporation section wick radial thermal resistance:

$$R_{Ew} = \frac{\ln(d_i/d_v)}{2\pi\lambda_e L_1} \qquad (7)$$

Vapor flow thermal resistance:

$$R_P = \frac{128 L_{eq}\mu_v T_v}{\pi d_v^{\,4}\rho_v^2 L^2} \qquad (8)$$

Condensation section wick radial thermal resistance:

$$R_{Cs} = \frac{\ln(d_i/d_v)}{2\pi\lambda_e L_2} \qquad (9)$$

Radial thermal resistance of the condensation section:

$$R_{Cw} = \frac{\ln(d_0/d_i)}{2\pi\lambda_w L_2} \qquad (10)$$

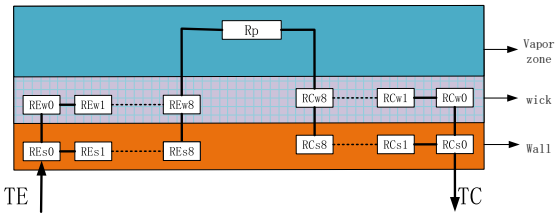

Fig. 6 Heat pipe heat resistance diagram

III.B. Thermoelectric conversion model

For the thermoelectric conversion device, a total of six thermoelectric conversion unites are distributed on the outer surface of the copper matrix. The hot junction of each TEG is in close contact with the copper matrix, while the cold junction is swiped away by seawater to remove waste heat. The thermoelectric conversion unit's control volumes are shown in the Figure 7, including the copper matrix, the insulating pads, and the TE cell. The heat conduction equations are respectively:

$$\nabla(k\nabla T) + \rho J^2 - TJ\left(\frac{\partial \alpha}{\partial T}\nabla T + (\nabla\alpha)_T\right) = 0 \qquad (11)$$

The terms, $\nabla(k\nabla T)$, ρJ^2 and $TJ\left(\frac{\partial \alpha}{\partial T}\nabla T + (\nabla\alpha)_T\right)$,in the equation represent the T.J. Seebeck effect, the Peltier effect and the Thomason effect.

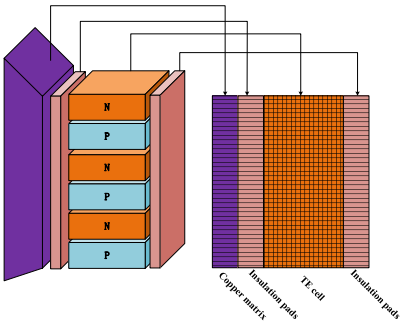

Fig. 7 Schematic of thermoelectric conversion model

IV. Steady state analysis

Figure 8 shows the radial temperature profile of six core channels, including the axial center position of the inlet and outlet reflectors. The highest temperature drop in the fuel pellet area is approximately 58 K. The fission gap also has considerable temperature differences. Compared to these two parts, the temperature difference in other areas is much smaller.

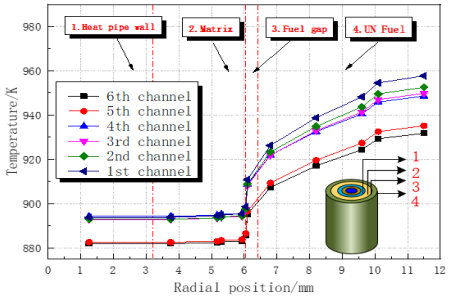

Fig. 8 Radial temperature distribution in different channel

Figure 9 shows the axial temperature distribution of the core average channel's multilayer structure substrate including the matrix, fuel gap and the fuel rods. It can be seen from the figure that the core block and the fuel gap temperature are highest at the axial center, which are about 938K and 893K (far below the temperature limit of the UN,2500K). The power and temperature of the fuel rod reach to peak due to the radial and axial reflection layers in the core. The temperature of matrix is substantially linear along the axial direction and the position of highest temperature is at the outlet of the core channel. Because the niobium-zirconium matrix has good thermal conductivity, the temperature distribution of core become more uniform, which is advantageous for the safety of the reactor system.

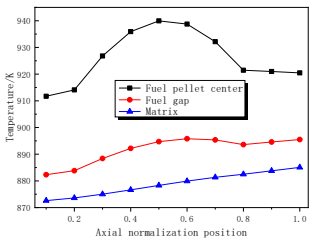

Fig. 9 Axial temperature distribution in different material

Figure 10 shows the axial temperature distribution of the heat pipes in different core channels which contains the temperature of wick. It can be seen that the temperature of the heat pipe's outer face wall is 5K higher than the temperature of the internal wick in the evaporation section. But the temperature of the wick structure is 0.7 K higher than the temperature of the wall when it reaches the condensation section for the reason why the length of the condensing section is longer than the length of the evaporating section. The axial temperature distribution of the heat pipe evaporation section covered by the core active zone is similar to the matrix temperature distribution. The axial temperature difference of the entire evaporation section has not exceeded 8k, and that in the condensation section is smaller even no temperature difference. It is the characteristic of the heat pipe that makes the core outlet temperature more uniform while ensuring the stability of the thermoelectric conversion device.

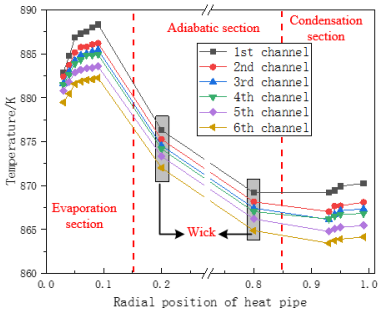

Fig. 10 Axial normalization heat pipe temperature distribution in different channel

Figure 11 is a temperature contour of thermoelectric conversion device, and the x-axis is along the direction of the seawater flow. The temperature distribution of the hot end of the thermoelectric conversion unit is relatively smooth because the heat pipe condensation section is isothermal. Since the inlet temperature of the coolant is close to seawater, the temperature at the cold junction of the thermocouple is lower at the coolant inlet and higher at the outlet. It can be seen that the temperature difference between cold and hot junction reaches 525k, which means that the efficiency will be 10.8% as shown in Fig.15.

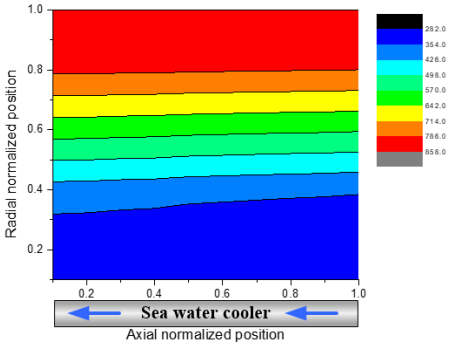

Fig. 11 Radial heat pipe temperature distribution in different channel

V. Summary and Conclusions

In this paper, a system analysis code is developed for micro nuclear reactor power system. The reactor neutronics and thermal–hydraulics models, the heat pipe model, the thermoelectric generator model and other components models are developed in this code. The following conclusions are drawn throughout this study:

(1) The system's steady-state calculations are performed on the designed micro-nuclear power source by using developed code.

(2) The temperature distribution of the fuel rod, the fuel gap, the matrix, the heat pipe and the thermoelectric conversion device.

(3) It is confirmed that the preliminary design of the thermoelectric conversion system and the residual heat removal system is reasonable and has sufficient safety margin to completely bring out the heat of the core.

REFERENCES

1. Li X, Wang Z. Unmanned Underwater Vehicle Technologies[J]. Marine Electric & Electric Technology, 2003.
2. Poston D I, Kapernick R J, Guffee R M. Design and anal-ysis of the SAFE-400 space fission reactor[C]// American Institute of Physics, 2002:578-588.
3. Poston D I. The heatpipe-operated Mars Exploration Reactor (HOMER)[J]. Office of Scientific & Technical Information Technical Reports, 2000.
4. Bushman A, Carpenter D M, Ellis T S, et al. The Martian Surface Reactor: An Advanced Nuclear Power Station for Manned Extraterrestrial Exploration[J]. 2004.
5. Tournier J, El‐Genk M S. Reactor Lithium Heat Pipes for HP‐STMCs Space Reactor Power System[C]// American Institute of Physics, 2004:781-792.
6. Wohlmuth R, Plettemeier D, Edenhofer P, et al. Radio Frequency Fluctuation Spectra during the Solar Conjunctions of the Ulysses, and Galileo, Spacecraft[M]// The 3-D Heliosphere at Solar Maximum. Springer Netherlands, 2001.
7. Toprak M, Stiewe C, Platzek D, et al. The Impact of Nanostructuring on the Thermal Conductivity of Thermoelectric CoSb3[J]. Advanced Functional Materials, 2010, 14(12):1189-1196.

Nomenclature:

t	time (s)
g	gravity (ms^{-2})
P	power (W)
C	delayed neutron precursor concentration (m^{-3})
Q	heat source ($W\ m^{-3}$)
D	diameter (m)
L	length (m)
T	temperature (K)
A	area (m^2)
q	heat flux ($W\ m^2$)
H	heat transfer coefficient ($W\ m^{-2}\ K^{-1}$)

Greek symbols

β	delayed neutron fraction
λ	heat conductivity ($W\ m^{-1}\ K^{-1}$) decay constant of precursors (s^{-1})
Λ	neutron generation time (s)
δ	wall thickness (m)
ρ	density (kg m3)
ε	emissivity
θ	angle (degree)

Subscripts

f	fission, fluid
U	fuel
G	gap
M	matrix
Es	evaporation section wall
Ew	evaporation section wick
Cs	condensation section wall
Cw	condensation section wall
W	wall